Research Square

Preprints are preliminary reports that have not undergone peer review.
They should not be considered conclusive, used to inform clinical practice,
or referenced by the media as validated information.

Zinc Metalloporphyrin-Modified Electrode for Electrochemical Sensing of Noradrenaline

Karen Kenlderi de Lima Augusto
karen.augusto@ufscar.br
Universidade Federal de São Carlos
Paulo Cardoso Gomes-Junior
Universidade Federal do Pará
Josias da Silveira Rocha
Universidade de São Paulo
Kleber Thiago de Oliveira
Universidade Federal de São Carlos
George Bueno Santana Pereira
Universidade Federal de Uberlândia
Orlando Fatibello-Filho
Universidade Federal de São Carlos

Research Article

Keywords: Noradrenaline, Zinc metalloporphyrin, Porphyrin sensor, Biological fluids, Electrochemical sensor, Differential pulse voltammetry

Posted Date: November 12th, 2026

DOI: https://doi.org/10.21203/rs.3.rs-11210963/v1

License: This work is licensed under a Creative Commons Attribution 4.0 International License.
Read Full License

Additional Declarations: No competing interests reported.

Zinc Metalloporphyrin-Modified Electrode for Electrochemical Sensing of Noradrenaline

Karen Kenlderi de Lima Augusto[1‡*], Paulo Cardoso Gomes-Junior[1,2‡], Josias da Silveira Rocha[1,3], Kleber Thiago de Oliveira[1], George Bueno Santana Pereira[1,4*], and Orlando Fatibello-Filho[1]

[1]*Departamento de Química, Universidade Federal de São Carlos, São Carlos, São Paulo, 13565-905, Brazil*

[2]*Faculty of Chemistry, Institute of Exact and Natural Sciences, Federal University of Pará, 66075-110, Belém, PA, Brazil*

[3]*Department of Chemistry, LABiQSC2 – Laboratory of Biological Activity and Supramolecular Chemistry of Coordination Compounds, Faculty of Philosophy, Sciences and Letters of Ribeirão Preto, University of São Paulo, Av. Bandeirantes, 3900, 14040-901, Ribeirão Preto, São Paulo, Brazil*

[4]*Instituto de Ciências Exatas e Naturais do Pontal, Universidade Federal de Uberlândia, Ituiutaba, Minas Gerais,* 38304-402*, Brazil*

‡These authors contributed equally to the work.

*Corresponding authors

E-mail addresses: karen.augusto@ufscar.br (Karen Kenlderi de Lima Augusto)

george.bsp@ufu.br (George Bueno Santana Pereira)

Abstract

Noradrenaline is an important catecholamine neurotransmitter involved in cardiovascular, neuroendocrine, and neuronal functions, and altered levels have been associated with pathological conditions. In this study, a zinc metalloporphyrin, mono-maleimide-tetraphenylporphyrinato-zinc(II), was combined with multi-walled carbon nanotubes to develop a modified glassy carbon electrode for the electrochemical detection of noradrenaline. The contribution of the zinc metalloporphyrin to the sensing interface was investigated by comparing zinc-containing and metal-free porphyrin systems. Incorporation of zinc resulted in a two-fold increase in anodic peak current and a reduction in charge-transfer resistance from 0.377 to 0.161 kΩ, indicating improved interfacial electron-transfer kinetics. Under optimised differential pulse voltammetry conditions, the modified electrode exhibited a linear response to noradrenaline from 1.0 to 84.2 μmol L^{-1}, with a detection limit of 0.26 μmol L^{-1}. The electrode also provided consistent recoveries of noradrenaline in spiked synthetic urine and bovine serum samples. These results demonstrate the functional contribution of the zinc metalloporphyrin to the carbon nanotube-based sensing interface and support its potential for electrochemical noradrenaline detection in complex samples.

Keywords: Noradrenaline; Zinc metalloporphyrin; Porphyrin sensor; Biological fluids; Electrochemical sensor; Differential pulse voltammetry.

1. Introduction

Electrochemical sensors are versatile devices widely used for the detection of diverse analytes. Their analytical performance can be enhanced through the incorporation of functional materials, particularly nanoparticles, which offer high electrical conductivity, large surface area, biocompatibility, and readily functionalised surfaces. These properties can promote electrocatalytic activity and facilitate the integration of additional functional components, enabling the development of tailored sensor architectures [1–5].

A class of materials that has gained prominence in electrochemical sensor development is porphyrins, heterocyclic compounds formed by four pyrrole subunits interconnected via methine bridges, resulting in versatile chelating systems [6]. They can bind metal ions, forming highly stable complexes; for instance, the stability constant for transition metal ions can reach values on the order of 10^{29} (*e.g.*, zinc-based metalloporphyrins). Furthermore, metalloporphyrins have rich redox chemistry because they can coordinate additional ligands above and below the porphyrin plane, making them promising compounds for electroanalytical applications [7].

In this regard, various studies in electrochemical sensors have exploited the porphyrins' characteristics to develop porphyrin-modified devices for detecting a wide range of analytes. Jemmeli *et al.* [8] prepared the (5,10,15,20-tetrakis[(4-methoxyphenyl)]porphyrinato)cadmium(II) ([Cd(TMPP)]) complex and used it to modify a carbon paste electrode to detect bisphenol A (BPA) in water samples. The sensor achieved a detection limit of 13.5 pM and the authors attribute the enhanced results for BPA electro-oxidation to the presence of [Cd(TMPP)], noting that the Cd metal centre enables more efficient electron transfer during BPA oxidation. Rejab *et al.* [9] developed a sensor using an indium-tin oxide (ITO) electrode modified with a zinc(II) metalloporphyrin complex, zinc(II) [5,10,15,20-tetrakis(2-methoxybenzene-4,1-diyl) tetraisonicotinate-porphyrinate] (ZnTMIPP), for selective glyphosate detection. The sensor exhibited a sensitive response to glyphosate, with a linear detection range of 10^{-8} to 10^{-5} M and a detection limit of 4.14 nM. Siddiqui *et al.* [10] developed an electrochemical sensor based on a zinc-tetramethoxyphenylporphyrin/carbon nanotube (ZnTMPP-CNT) composite to modify a glassy carbon electrode for detecting 5-fluorouracil in real human blood serum samples. The ZnTMPP-CNT/GCE sensor exhibited a linear response in the ranges of 0.1 – 1.0 μM and 2.0 – 14.0 μM, with limits of detection and quantification of 0.098 μM and 0.327 μM, respectively.

Porphyrins have also been used in sensor architectures to detect neurotransmitters, endogenous molecules that transmit electrical impulses from one nerve cell to another nerve, muscle, organ, or other tissues, acting as messengers of neurological information, making them

important targets as their concentrations can provide information on physiological processes and their dysregulation may be associated with pathological conditions [11]. Askri *et al.* [12] developed an electrochemical sensor based on a GCE modified with a manganese(III) porphyrin complex, (triflate)[(meso-tetra(p-tolylphenyl)porphyrinato)]manganese(III), to detect serotonin in synthetic urine. The $[Mn^{III}(TTP)(SO_3CF_3)]$/GCE sensor exhibited a detection limit of 5.3 μM and a linear range of 10 – 250 μM. The authors attribute the enhanced electrocatalytic activity and improved electron-transfer efficiency to the increased content of $[Mn^{III}(TTP)(SO_3CF_3)]$, which allows greater availability of active sites and better interaction between the analyte and the electrode surface. Ma *et al.* [13] developed an electrochemical sensor based on a bimetallic Co/Zn porphyrin metal-organic framework (MOF) for dopamine (DA) detection. Metal-ion doping improved the pore environment and increased the variety and spatial arrangement of the MOF's active sites, facilitating electron transfer and exchange with DA. Furthermore, the Co^{2+} and Zn^{2+} active centres exert a synergistic effect, significantly enhancing the MOF's catalytic activity; The sensor exhibited a linear range of 5 nM – 177.8 μM and a detection limit of 1.67 nM for DA detection.

Among neurotransmitters, noradrenaline (NE) is a catecholamine neurotransmitter that plays an important role in the regulation of cardiovascular, neuroendocrine, and neuronal functions [14]. Altered NE levels have been associated with pathological conditions involving catecholamine imbalance, particularly catecholamine-secreting tumours such as pheochromocytoma and paraganglioma [15,16]. In such conditions, elevated NE concentrations have been reported in biological fluids, including urine and serum. Reported urinary NE concentrations range from approximately 0.12 μM (subclinical phaeochromocytoma, within the normal excretion range; in this case, nearly identical NE excretion of 402 and 378 nmol day^{-1} corresponded to 0.26 and 0.12 μM solely because of different urine volumes, 1.52 and 3.10 L, illustrating the influence of hydration on urinary concentration) to 6.0 μM (overt phaeochromocytoma with acute heart failure) [17,18]. Serum NE concentrations are typically in the low nanomolar range; however, substantially elevated levels may occur under severe pathological conditions. In a reported case of phaeochromocytoma multisystem crisis, in which the patient had also received exogenous noradrenaline for shock, serum NE reached 72,212 pg mL^{-1} (approximately 0.43 μM) [19]. Therefore, the development of sensitive analytical approaches for NE determination is of interest for the assessment of altered catecholamine levels in biological samples.

Hence, the development of sensitive analytical approaches for NE detection is of interest for the assessment of altered noradrenaline levels in biological samples. In this study, we investigate the electrochemical performance of the zinc metalloporphyrin {5-[4-(2,5-dioxo-2,5-

dihydro-1H-pyrrol-1-yl)]-5,10,15,20-tetraphenylporphyrinato}zinc(II), commonly referred to as (mono-maleimide-tetraphenylporphyrinato)zinc(II) (ZnMMTPP), combined with multi-walled carbon nanotubes (MWCNTs) for the detection of noradrenaline. The resulting ZnMMTPP-MWCNT-modified glassy carbon electrode was evaluated for the electrochemical detection of NE, including its analytical performance in biological matrices.

2. Experimental

2.1. Chemicals and Solutions

All chemicals were of analytical grade. Dichloromethane, benzaldehyde, pyrrole, BF_3-etherate, DDQ (2,3-dichloro-5,6-dicyano-1,4-benzoquinone), $NaHCO_3$, $Zn(CH_3CO_2)_2 \cdot 2H_2O$, hexanes, methanol, toluene, ethyl acetate, $CDCl_3$, noradrenaline tartrate (NE, pharmaceutical primary standard), bovine calf serum (sterile-filtered, hemoglobinv ≤35 mg/dL), and multi-walled carbon nanotubes (MWCNTs; outer diameter × length: 6-9 nm × 5 μm; >95 % carbon) were acquired from Sigma Aldrich (St. Louis, USA). Pyrrole, dichloromethane, and BF_3-etherate were purified by distillation. Potassium phosphate monobasic (≥ 99 %) and potassium phosphate dibasic (≥ 99 %) were acquired from Synth (Diadema, São Paulo). All solutions were prepared with ultrapure water (resistivity ≥18.0 MΩ cm) obtained from a Millipore Milli-Q system (Billerica, USA).

A 0.20 mol L^{-1} phosphate solution (pH 5.0) was used as the supporting electrolyte, with pH adjustments (5 to 9) made using 1.0 mol L^{-1} NaOH. A 1.0×10^{-2} mol L^{-1} standard stock solution of noradrenaline (NE) was prepared in the same buffer, and dilutions were performed to obtain solutions of varying concentrations. Potential interferents, including urea, glucose, ascorbic acid, dopamine, caffeine, uric acid, and common ions such as chloride, sodium, potassium, and sulphate were assessed for their influence on NE detection by the proposed method.

2.2. Apparatus

The spectra in the visible ultraviolet region were obtained using a SHIMADZU UV-1650PC spectrophotometer. The characterizations of the complexes were performed in dichloromethane 3×10^{-6} mol L^{-1}, using quartz cuvettes with an optical path of 1 cm, and the scan was performed in the region from 750 to 300 nm. The spectra were obtained and processed using UVProbe 2.42. The blank was subtracted using a second beam of light during the experiments. The ^1H nuclear magnetic resonance spectra were obtained using the Bruker 9.4 Tesla spectrometer (400 MHz for hydrogen frequency). The IR samples were analysed using SHIMADZU IRPrestige-21 equipment with CsI pellets. The spectra were collected with 64 scans for greater accuracy in a scan range of 4000 to 240 cm^{-1}, with a resolution of 4 cm^{-1}. The spectra were obtained and the baseline corrected using the Shimadzu IRsolution 1.60 program. The compounds were analysed using a high-resolution mass spectrometer with electrospray ionisation (HRMS-ESI) in the positive mode using an Agilent LC-6545 Q-TOF-MS mass spectrometer (Agilent Technologies, Santa Clara, CA, EUA). The spectra were acquired by

monitoring a range between 100 and 1,500 Da and processed by MassHunder Workstation software version B.08.00.

Morphological characterisation of the composite films was carried out using field-emission scanning electron microscopy (FEG/SEM, FEI Magellan 400 L) and transmission electron microscopy (TEM, FEI Tecnai G2 F20, operated at 200 kV). In addition, atomic force microscopy (Bruker Nanoscope 6 Multimode 8) was employed to analyse surface topography and roughness.

Electrochemical analysis of noradrenaline was carried out using a PGSTAT101 potentiostat/galvanostat (Metrohm Autolab, Utrecht, Netherlands), with data acquisition and processing performed with NOVA 2.1.7 software. Electrochemical impedance spectroscopy (EIS) measurements were conducted using a Sensit Smart potentiostat (PalmSens, the Netherlands) in the frequency range from 65 kHz to 0.1 Hz, an AC amplitude of 10 mV was applied to perturb the system. Data were recorded using PStrace 5.9 software, and Nyquist plots were fitted to appropriate equivalent circuits using ZView 2.0 software.

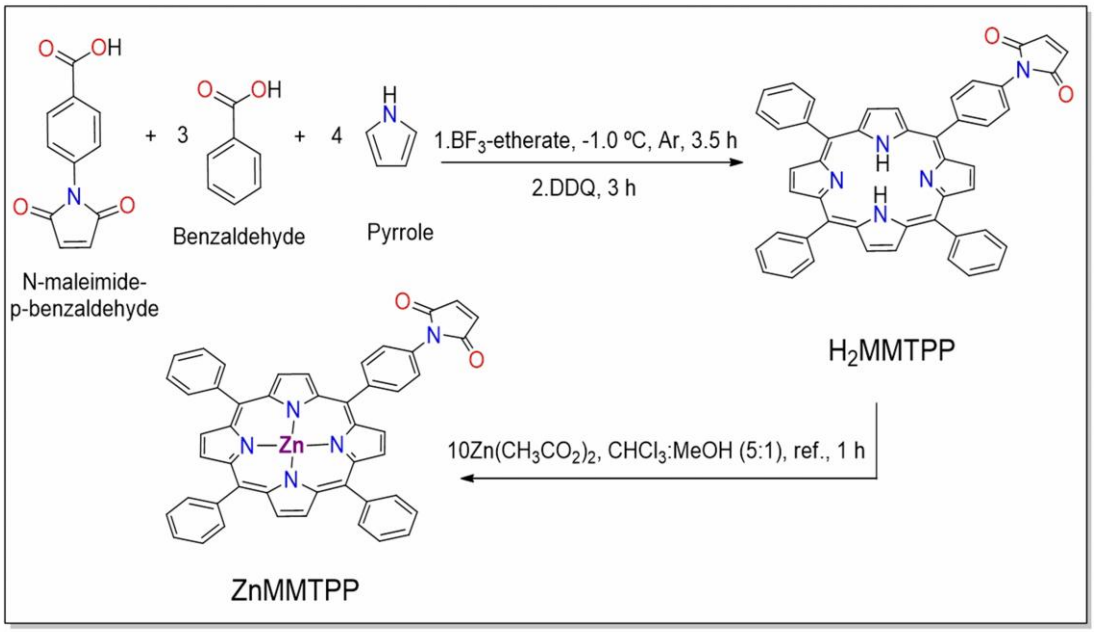
Electrochemical measurements were performed using a conventional three-electrode cell, comprising a platinum plate (1.0 cm^2) as the counter electrode, an Ag|AgCl (3.0 $mol \cdot L^{-1}$ KCl) reference electrode, and a glassy carbon electrode (GCE, Ø 3.0 mm) as the working electrode. The catalytic rate constant (k_{cat}) for noradrenaline at the modified electrode was determined by chronoamperometry, applying a fixed potential of +0.22 V with a time interval of 0.01 s.

2.3. Preparation of H_2MMTPP and ZnMMTPP Porphyrins

H_2MMTPP: The 5-[4-(2,5-dioxo-2,5-dihydro-1H-pyrrol-1-yl)]-5,10,15,20-tetraphenylporphyrin, usually referred in this paper as mono-maleimide-tetraphenylporphyrin (H_2MMTPP), was synthesized according to methods adapted from the literature [20]. In a 250 mL two-necked flask, 200 mL of dichloromethane, 4-N-maleimidyl-p-benzaldehyde (100.04 mg, 0.50 mmol), benzaldehyde (153.0 µL, 1.5 mmol), and pyrrole (139.0 µL, 2.00 mmol) were added. This solution was degassed with argon and cooled to –1 °C for 10 minutes. After this period, BF_3-etherate (70 µL, 0.539 mmol) was added and the reaction medium was kept under an inert atmosphere. Aliquots were taken from the reaction and monitored by UV-visible spectroscopy, with the porphyrin being revealed with a solution of DDQ (2,3-dichloro-5,6-dicyano-1,4-benzoquinone). Then, the reaction was maintained for 3.5 h, and then DDQ (1.50 mmol, 340.80 mg) was added, and the reaction medium was kept under stirring for 3 h at room

temperature. Afterwards, the reaction was purified by 10 x 50 mL liquid-liquid extraction with a cold 2 % $NaHCO_3$ solution. Finally, the product was purified by flash column with toluene: ethyl acetate (9:1) eluent. Yield: 11 % (0.055 mmol, 39.5 mg) (Scheme 1). ^{1}H NMR (400 MHz, $CDCl_3$): δ (ppm) = -2.78 (s, 2H, N-H); 7.02 (s, 2H, H_M); 7.74-7,80 (m, 9H+2H, H_p/H_o + H_2); 8.22-8.24 (m, 6H, H_m); 8.31-8.33 (m, 2H, H_1) 8.85-8.89 (m, 8H, H-β). UV-vis in CH_2Cl_2 λ [nm]: 425, 522, 560, 597, 660. HRMS (ESI, positive mode), $[M+H]^+$: found 710.2591, cal. 710.2550.

ZnMMTPP: The {5-[4-(2,5-dioxo-2,5-dihydro-1H-pyrrol-1-yl)]-5,10,15,20-tetra-phenylporphyrinato}zinco(II), usually referred in this paper as (mono-maleimide-tetra-phenylporphyrinato)zinco(II) (ZnMMTPP), was synthesized according to methods adapted from the literature [21]. H_2MMTPP (10.1 mg, 14.1 µmol) was dissolved in 2.5 mL of dichloro-methane at room temperature. Then, $Zn(CH_3CO_2)_2.2H_2O$ (31.0 mg, 141.0 µmol) solubilized in 0.5 mL of methanol was added, and the reaction medium was kept under reflux with magnetic stirring during 1 h. After this period, 10.0 mL of hexanes were added, then the solid was filtered and washed with 20.0 mL of distilled water, 20 mL of methanol, and 20 mL of ethyl ether. Subsequently, the product was dried under vacuum, obtaining the complex ZnMMTPP (Scheme 1). Yield: 77 % (8.7 mg, 11.25 µmol). ^{1}H NMR (400 MHz, $CDCl_3$): δ (ppm) = 7.03 (s, 2H, H_M); 7.73-7.81 (m, 9H+2H, H_p/H_o + H_2); 8.22-8.24 (m, 6H, H_m); 8.31-8.34 (m, 2H, H_1) 8.95-8.90 (m, 8H, H-β). UV-vis in CH_2Cl_2 λ [nm]: 419, 511, 548, 586. HRMS (ESI, positive mode), $[M+H]^+$: found 772.1685, cal. 772.1711.



Scheme 1. Synthesis of the ZnMMTPP porphyrins.

2.4. Preparation of Glassy Carbon Electrodes Modified with Porphyrins

In this study, the GCE was modified using a suspension containing porphyrins (H_2MMTPP or ZnMMTPP) and MWCNT. Prior to modification, the GCE surface was polished with 0.5 µm alumina slurry and rinsed thoroughly with deionised water. The modifying suspensions were prepared by dispersing 1.0 mg of MWCNT and 1.0 mg of either ZnMMTPP or H_2MMTPP in 980 µL of N,N-dimethylformamide (DMF) and 20 µL of Nafion™. The mixtures were sonicated for 30 minutes in an ultrasonic bath to ensure homogeneous dispersion. Subsequently, 10.0 µL of the suspension was drop-cast onto the GCE surface and left to dry in a desiccator for approximately 2 hours to form a stable film.

2.5. Synthetic Urine and Bovine Serum Preparation

Synthetic urine samples were prepared following the procedure described by Laube et al. [22], consisting of 0.20 mmol L^{-1} KCl, 0.18 mmol L^{-1} NH_4Cl, 0.10 mmol L^{-1} NaCl, 0.10 mmol L^{-1} $CaCl_2$, 0.15 mmol L^{-1} KH_2PO_4, and 0.18 mmol L^{-1} urea in a 25 mL volumetric flask. These samples were spiked with three concentrations of NE (2.0, 8.0, and 25.0 µmol L^{-1}), and the corresponding recovery percentages were calculated. Similarly, bovine serum samples were diluted 50-fold with ultrapure water, spiked with the same concentrations of NE, and evaluated by determining the recovery rates.

3. Results and Discussion

3.1. Preparation and Characterisation of ZnMMTPP and H_2MMTPP Porphyrins

The absorption spectra of free porphyrins show a band of higher molar absorptivity around 410 to 430 nm, called the Soret band, related to the $S_0 \rightarrow S_2$ transition and four bands of lower molar absorptivities between 514 to 645 nm named Q bands and associated with $S_0 \rightarrow S_1$ transitions. After coordination with zinc, a change is noted in these Q bands, characteristic of coordination due to the increase of symmetry of the metalloporphyrin when compared to the same free porphyrin (Figures S1, S2 and S3).

^{1}H nuclear magnetic resonance spectroscopy is a technique that proves the aromatic nature of porphyrins [23]. For example, imine hydrogens are normally observed in a highly shielded region of the ^{1}H NMR spectrum, at −2.78ppm for H_2MMTPP compared to the TMS signal. Figure S4. This characteristic proves that the shielding of these protons is related to the anisotropic effect, which is further evidence of the high aromaticity of porphyrins. From the NMR spectrum of the [Zn(MMTTP)] complex, the disappearance of the signal referring to imine hydrogens was verified, characterizing the formation of zinc(II) metalloporphyrin [23], Figure S5.

Electron spray ionization mass spectrometry (ESI-MS) is an important tool for determining the molecular mass of the ion/ion charge (m/z) and the isotopic pattern of organometallic and coordination compounds [24]. The molecular ion detected in free porphyrin and in the [Zn(H_2MMTTP)] complex was $[M+H]^+$. Where the peaks of the molecular ions are $[710.2591+H]^+$ and $[772.1711+H]^+$, respectively. Demonstrating the success in obtaining the compounds synthesized here. The isotopic patterns can be seen in the SI, Figures S6 and S7.

This same behavior, *i.e.*, the loss of imine hydrogens after coordination, is evident in the infrared spectrum. For H_2MMTTP, a band was observed at 3309 cm^{-1}, related to the νN-H stretching and νC=O (1709 cm^{-1} from pyrrole substituent). The absence of such a band in the Zn compound demonstrates the disappearance of this bond, indicating the formation of complexes. Additionally, another important characteristic of metalloporphyrins when compared to free porphyrins is the appearance of a single band around 1004 cm^{-1}, related to the stretching of the nitrogen-metal bond out of plane (νNP-M), core porphyrin, or also called pyrrole breathing (πP), this is characteristic of the increase in symmetry of the system, as also evidenced by UV-Vis [23], Figure S8.

3.2. Electrochemical Behaviour of Noradrenaline at Porphyrin-Modified Glassy Carbon Electrodes

The proposed electrodes were electrochemically characterised using 100 µM noradrenaline (NE) in phosphate solution (pH 5.0) by cyclic voltammetry (CV) and electrochemical impedance spectroscopy (EIS). All electrochemical studies, including CV, EIS, and scan rate analyses, were performed on bare GCE, MWCNT/GCE, H_2MMTPP-MWCNT/GCE, and ZnMMTPP-MWCNT/GCE, as presented in Figure 1, Figures S9 and S10, and Table 1. The performance of each electrode can be assessed by comparing key parameters such as the anodic peak current (I_{ap}), peak-to-peak separation (ΔE_p), electroactive area (A_e) (Equations S1 and S2), charge transfer resistance (R_{ct}), apparent electron transfer rate constant (k_{app}, Equation S3), and parameters derived from the constant phase element (capacitance and α).

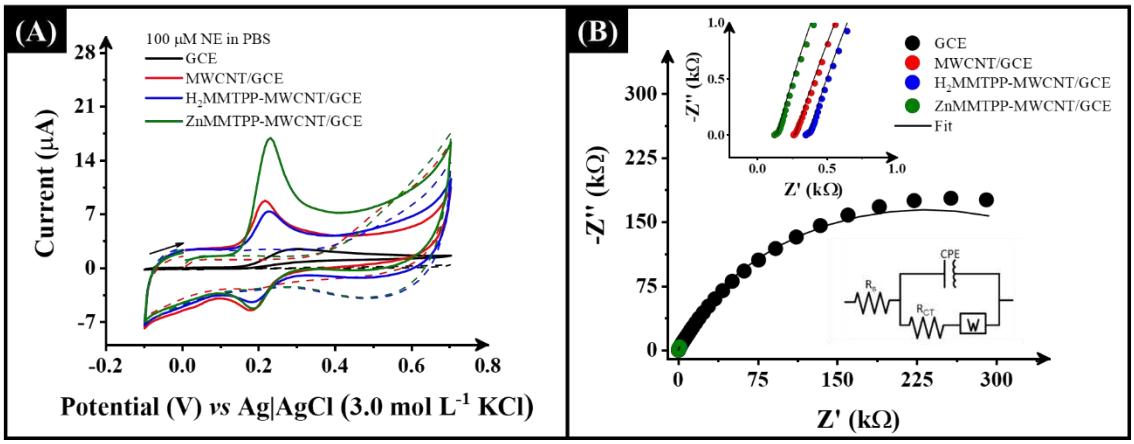
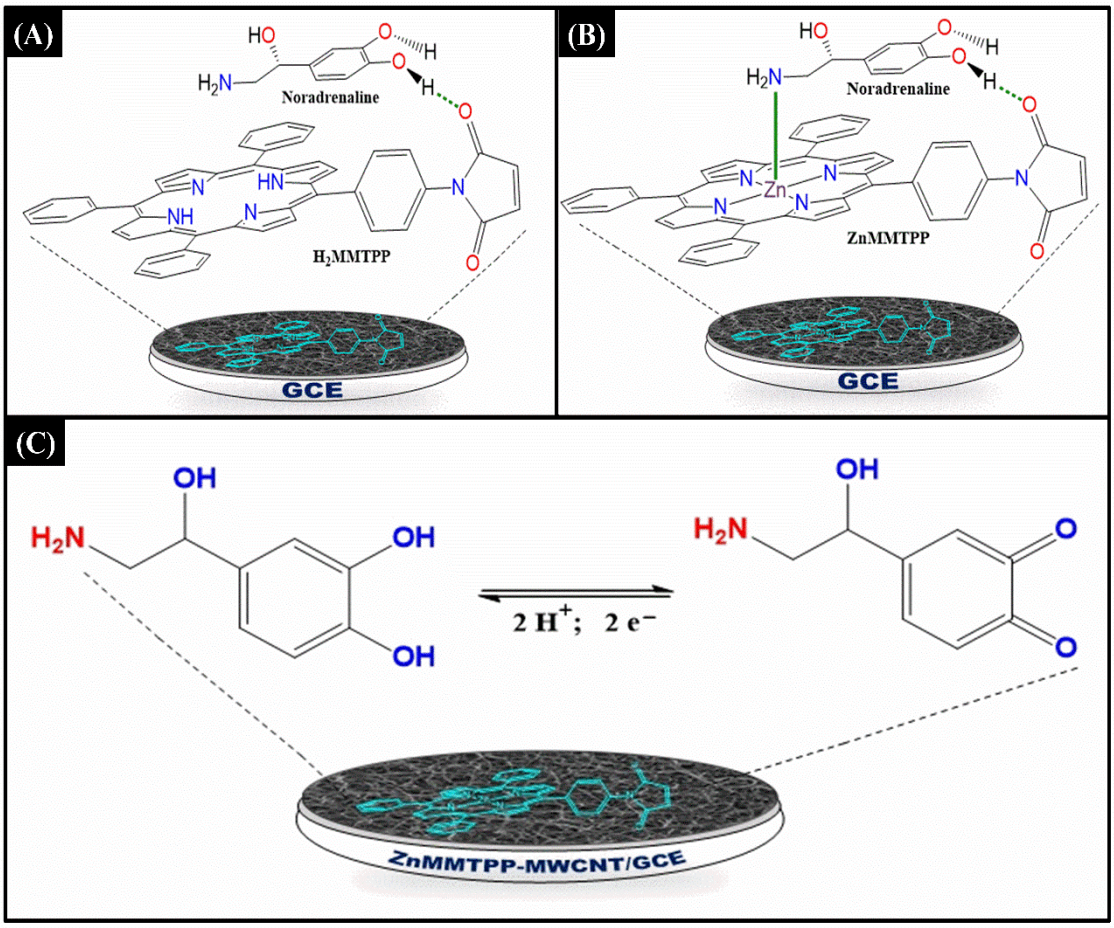


Figure 1. (A) CVs (50 mV s^{-1}) and (B) Nyquist plots using GCE, MWCNT/GCE, H_2MMTPP-MWCNT/GCE and ZnMMTPP-MWWCNT/GCE as the WE in 100 µM NE in 0.2 mol L^{-1} phosphate solution (pH 5.0). Inset (B): the proposed equivalent circuit.

The bare GCE, as expected, showed the lowest I_{ap} and the smallest electroactive area, along with a very high charge transfer resistance (46.7 kΩ) and the lowest k_{app} (5.7×10^{-6} cm s^{-1}), indicating sluggish electron transfer kinetics and poor electrochemical performance. Upon modification with MWCNTs, there is a substantial enhancement in I_{ap} and a significant increase in A_e accounting for an increase of 3.6- and 27-fold, respectively. Moreover, it was observed a remarkable decrease in R_{ct} to 0.306 kΩ accompanied by an increase in k_{app} to 8.7×10^{-4} cm s^{-1}. The decreased ΔE_p highlights the conductive and catalytic role of MWCNTs in facilitating the electron transfer [25]. Further functionalisation with H_2MMTPP slightly reduced the current response (7.33 µA) and k_{app} compared to MWCNT/GCE, possibly due to the partial blocking of active sites or less efficient NE interactions mediated by the maleimide-containing porphyrin layer, which may not favour charge transfer (Scheme 1A). However, the electroactive area

remains comparable (1.02 cm^2), and R_{ct} shows only a moderate increase (0.377 kΩ), indicating that the film still maintains relatively good conductivity.

On the other hand, the Zn porphyrin (ZnMMTPP) in combination with MWCNTs yields the best overall electrochemical performance. The ZnMMTPP-MWCNT/GCE electrode exhibits the highest I_{ap}, with improvement of 6.9-fold and about 2-fold for ZnMMTPP-MWCNT/GCE compared to GCE and MWCNT/GCE H_2MMTPP-MWCNT/GC electrodes, significantly reduced R_{ct} (0.161 kΩ), and the highest k_{app} value (1.7×10^{-3} cm s^{-1}), demonstrating that Zn coordination enhances the electron-donating ability of the porphyrin and improves the electron transfer efficiency. Although its electroactive area is slightly lower than that of the H_2MMTPP-modified electrode, the lower R_{ct} and higher k_{app} indicate superior charge transfer kinetics. Furthermore, the Zn porphyrin significantly improves charge transfer, possibly due to the redox-mediation properties of the Zn(II) centre, which enhance electron exchange between noradrenaline and the electrode surface, as shown in Scheme 2B. Reports from the literature indicate that porphyrin-based sensors exhibit enhanced voltammetric responses for the target analyte, due to metal centres functioning as effective mediators for electron transfer [26,27] .



Scheme 2. Illustration of H_2MMTPP-MWCNT/GCE (A) and ZnMMTPP-MWCNT/GCE (B), highlighting the role of ZnMMTPP in enhancing charge transfer. In (C) suggested electrochemical mechanism for noradrenaline oxidation at the ZnMMTPP-MWCNT/GCE electrode.

Regarding EIS fitting parameters, the α values (indicative of surface homogeneity) [28] range between 0.70 and 0.80 for the modified electrodes, suggesting relatively uniform surfaces. The χ^2 values are all low, confirming good fitting quality. Overall, the incorporation of MWCNTs greatly enhances the electrochemical response of GCEs, and further modification with porphyrins, especially ZnMMTPP, significantly enhances the performance, making ZnMMTPP-MWCNT/GCE a promising electrode for sensitive noradrenaline detection.

Table 1. Electrochemical and EIS data extracted from Figure 1 using 100 µM NE (in phosphate solution (pH 5.0)

Electrode	I_{ap} (µA)	ΔE_{ap} (mV)	A_e (cm^2)	R_{ct} (kΩ)	k_{app} (cm s^{-1})	CPE (µF $s^{\alpha-1}$)	α	χ^2
Bare GCE	2.44	—	0.04	46.7	5.7×10^{-6}	2.2	0.78	0.26
MWCNT/GCE	8.74	37	1.07	0.306	8.7×10^{-4}	499	0.71	0.04
H_2MMTPP-MWCNT/GCE	7.33	44	1.02	0.377	7.1×10^{-4}	20.7	0.80	0.04
ZnMMTPP-MWCNT/GCE	16.90	44	0.86	0.161	1.7×10^{-3}	393	0.70	0.05

Further analysis of Figures S9 and S10, which present the results of potential scan rate studies, reveals an irreversible electrochemical behaviour of noradrenaline at the bare GCE. In contrast, the modified electrodes exhibited *quasi*-reversible behaviour, indicating improved electron transfer kinetics. This observation aligns with the previously discussed enhancement provided by the electrode modifications (MWCNT, H_2MMTPP-MWCNT, and ZnMMTPP-MWCNT), which facilitate the redox process of NE. For the unmodified GCE, the electrochemical response of NE was diffusion-controlled, as evidenced by the linear relationship between peak current and the square root of the scan rate, as well as the slope of 0.36 obtained from the log (I_{ap}) *vs* log (v) plot [29]. In contrast, the modified electrodes demonstrated adsorption-controlled behaviour, likely due to strong interactions between NE and the nanostructured materials. These interactions can promote pre-concentration of the analyte at the electrode surface. Furthermore, the presence of functional groups in both the MWCNTs and porphyrin structures may enhance these interactions, contributing to the observed adsorptive behaviour.

To assess the interaction levels between NE and the porphyrin-derived active sites, CV analysis was used to determine the specific Faradaic capacitance (C_S) of the MWCNT/GCE, H_2MMTPP-MWCNT/GCE, and ZnMMTPP-MWCNT/GCE during NE electrooxidation. This may indicate catalytic improvements due to ZnMMTPP's ability to store charge during the Faradaic reaction, compared with the other electrodes. Accordingly, Equation 1 was employed in the proposed model, utilising data obtained from the CV analysis.

$$C_s = \frac{A}{2\Delta V m v} \quad \textbf{Equation 1}$$

where C_s is the specific faradaic capacitance (F g^{-1}), A is the integrated area of the cyclic voltammogram (A V), m is the mass of the active material (g), v is the scan rate of CV (V s^{-1}), and ΔV is the potential window of the CV (total voltage range). The integrated area values obtained for the NE CVs are shown in Figure S11. The C_s values were 67, 63, and 84 mF g^{-1} for the MWCNT/GCE, H_2MMTPP-MWCNT/GCE, and ZnMMTPP-MWCNT/GCE, respectively. These results suggest that the zinc-containing porphyrin enhances the faradaic response to NE, consistent with the EIS results showing an increased double-layer capacitance and facilitated interfacial charge transfer. This increase is attributed to the interaction of NE with the porphyrin's metal centre, which contribute to its catalytic activity and the analyte's adsorptive effect on the electrode surface.

3.3. Physical Characterization of the Electrode

The topographical analysis using AFM (Figure 2A and B and Figure S12A) reveals substantial morphological differences among the electrodes modified with MWCNT, H_2MMTPP-MWCNT, and ZnMMTPP-MWCNT. The MWCNT composite film surface exhibits pronounced roughness with sharp peaks reaching up to 117 nm, characteristic of aggregated carbon nanotubes. Upon functionalisation with H_2MMTPP, the surface becomes significantly more compact and uniform, with a maximum height of only 17 nm and an root mean square (RMS) roughness of 2.35 nm, indicating effective surface coverage and improved nanotube dispersion (Figure S12A). In comparison, the ZnMMTPP-MWCNT composite film presents intermediate characteristics: the maximum height is 95 nm and the RMS value increases slightly to 3.65 nm. This suggests that the presence of the central zinc ion in ZnMMTPP affects the packing and organisation of the porphyrin layer on the nanotube surface. While both porphyrin modifications reduce surface roughness relative to bare MWCNTs, the metal-free porphyrin leads to a smoother and more compact morphology. The slightly higher roughness observed with ZnMMTPP may be associated with electronic effects introduced by the zinc centre, potentially influencing molecular orientation and self-assembly on the carbon surface. These morphological changes are expected to improve charge transfer processes and contribute to the enhanced electrochemical behaviour of the modified electrode.

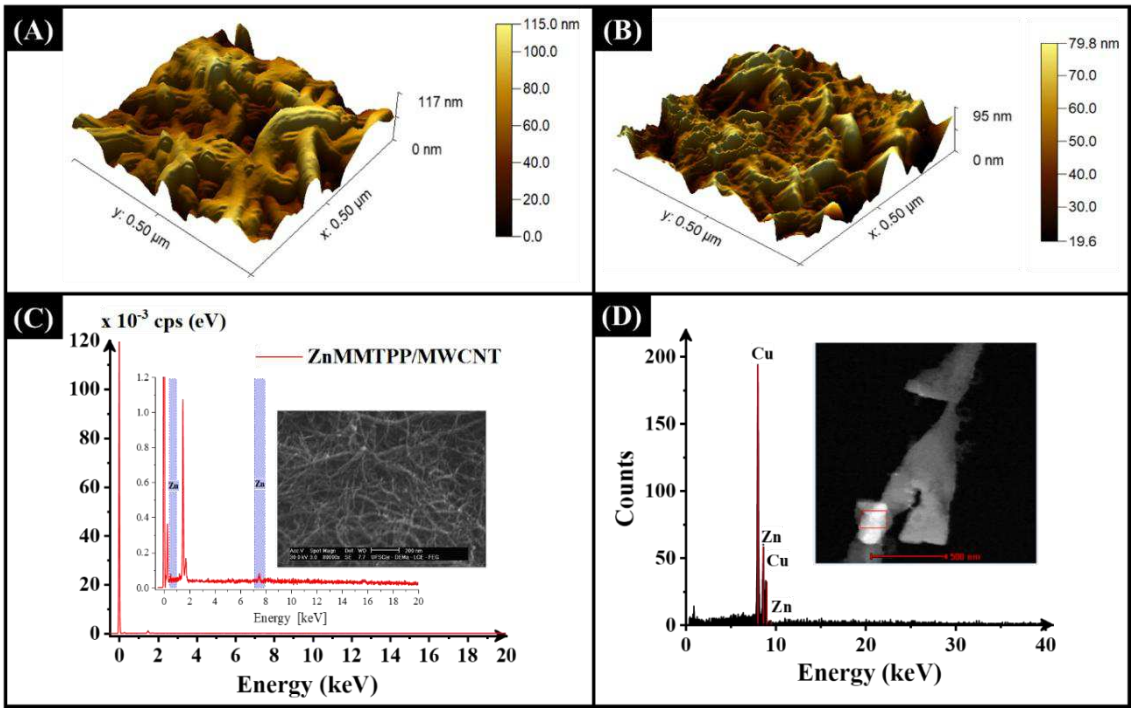


Figure 2. 3D AFM topography images for (A) MWCNT suspension and (B) ZnMMTPP-MWCNT suspension. (C) EDS spectrum and SEM images and (D) EDS spectrum and TEM image obtained for ZnMMTPP-MWCNT composite film.

Following the initial characterisation, the composite film containing ZnMMTPP-MWCNT and the suspension with only MWCNT were further analysed using SEM/EDS and TEM, as shown in Figure 2C and D and Figure S12B. The EDS spectrum in Figure 2C displays the emission lines at 0.5 and 7.5 keV, characteristic optical absorption peaks attributed to Zn in the porphyrin in the selected SEM micrograph, confirming the incorporation of ZnMMTPP into the ZnMMTPP-MWCNT composite film. In Figure S12B, the EDS analysis reveals the presence of oxygen, which is associated with MWCNT surface functional groups such as hydroxyl (OH) and carbonyl (O–C=O) [25]. In both micrographs, the typical cylindrical morphology of carbon nanotubes is clearly observed. In Figure 2D, the energy-dispersive X-ray (EDX) spectrum of the porphyrin reveals Zn emission lines; these characteristic peaks (between 8.6 and 9.5 keV) suggest the presence of the metal within the porphyrin structure. These findings corroborate the UV-Vis, NMR, FTIR, and mass spectrometry results, confirming the successful synthesis of ZnMMTPP (the inset in Figure 2D highlights the analysed region). Furthermore, the TEM image in the inset of Figure 2D shows that the porphyrin exhibits an irregular morphology, and Figure S12C displays a selected-area electron diffraction (SAED) pattern that demonstrates the crystalline phase of ZnMMTPP.

3.4. Kinetics of Noradrenaline at Modified Electrodes

The catalytic rate constant (k_{cat}) for the reaction between noradrenaline in 0.2 mol L^{-1} phosphate solution (pH 5.0) and the redox-active sites of the ZnMMTPP-MWCNT film on the GCE was determined by chronoamperometry using the ZnMMTPP-MWCNT/GCE. For comparison, the same parameter was also evaluated for the unmodified GCE and the MWCNT/GCE. The k_{cat} values were calculated based on chronoamperometric data using Equation 2 [30]:

$$\frac{I_{cat}}{I_L} = (\pi k_{cat} C t)^{1/2} \quad \textbf{Equation 2}$$

In Equation 2, I_{cat} represents the catalytic current in the presence of NE, I_L is the current in its absence, C is the bulk concentration of NE (100 μM), k_{cat} is the catalytic rate constant (L mol^{-1} s^{-1}), and t is the elapsed time (s). The catalytic rate constant was determined from the slope of the I_{cat}/ I_L *vs* $t^{1/2}$plot (Figure S13). The calculated k_{cat} values were 4.5×10^1 L mol^{-1} s^{-1}, 8.2×10^4 L mol^{-1} s^{-1}, and 4.2×10^5 L mol^{-1} s^{-1} for GCE, MWCNT/GCE, and ZnMMTPP-MWCNT/GCE, respectively. The k_{cat} value obtained using the ZnMMTPP-MWCNT/GCE was higher than those previously reported in the literature for noradrenaline [31–33], indicating enhanced catalytic efficiency. This improvement is attributed to the synergistic effect between the Zn-porphyrin complex and the MWCNTs, which facilitates electron transfer and promotes the electrochemical oxidation of noradrenaline at the electrode surface.

3.5. Electroanalytical Determination of Noradrenaline

To investigate the pH dependence of noradrenaline oxidation, differential pulse voltammetry (DPV) was performed using 100 μmol L^{-1} NE in 0.2 mol L^{-1} Britton-Robinson (BR) buffer over the pH range of 5.0 to 9.0 (Figure S14A). As shown in Figure S14B, a linear shift in anodic peak potential towards more negative values was observed with increasing pH (pH 5.0 to 8.0). The slope of the E_{ap} *vs* pH plot was 55 mV pH^{-1}, indicating that the oxidation process involves an equal number of protons and electrons, consistent with literature reports, which attribute two electrons to the oxidation of NE (Scheme 2C) [31,34–36]. The inset in Figure S13A displays the relationship between anodic peak current and pH, revealing a maximum current at pH 5.0, followed by a gradual decrease at higher pH values. Based on this behaviour, pH 5.0 was selected for subsequent measurements. Additionally, the effect of different supporting electrolytes (Figure S14C) at pH 5.0 was evaluated by comparing 0.2 mol L^{-1} phosphate solution and BR buffer. Phosphate solution provided the highest peak current and was therefore chosen as the supporting electrolyte for further experiments.

To enhance the determination of NE, the DPV parameters were optimised. Table S1 presents the results of the optimisation of amplitude (a), modulation time (t_m), interval time, (t), and potential increment (ΔE), based on the oxidation response of noradrenaline at the proposed electrode. The optimal DPV conditions, determined based on the oxidation response of NE at the ZnMMTPP-MWCNT/GCE electrode, were a pulse amplitude of 100 mV, a potential increment of 3 mV, interval time of 150 ms, and a modulation time of 40 ms. Under the optimised conditions, an analytical calibration curve for NE oxidation was constructed over the concentration range of 1.0 to 84.2 µmol L^{-1}. Figure 3A and B displays the corresponding DP voltammograms and the resulting linear calibration plot for this range, respectively. The limit of detection (LOD) was calculated using the equation LOD = 3σ/slope, where σ is the standard deviation of 10 blank measurements (0.2 mol L^{-1} phosphate solution, pH 5.0).

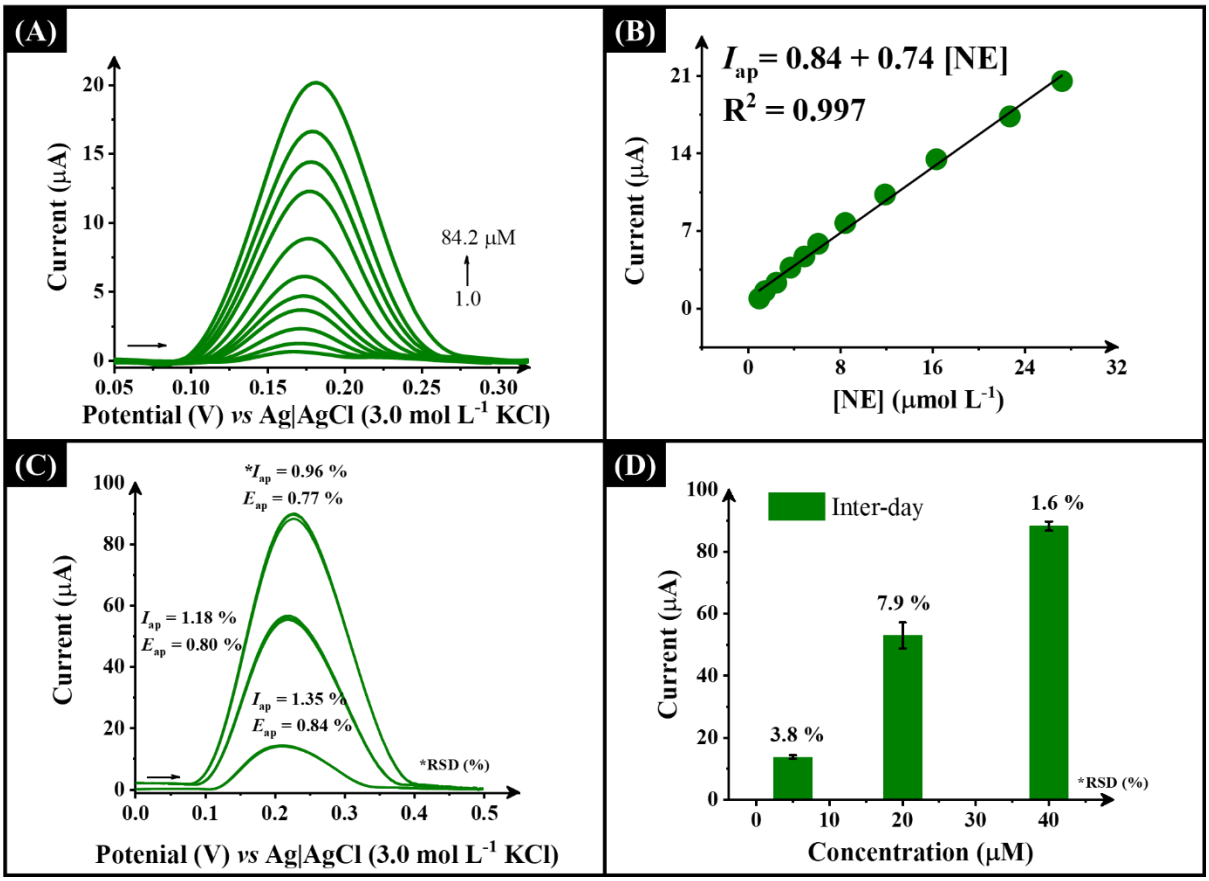


Figure 3. (A) DP voltammograms in the presence of different concentrations of NE (1.0 to 84.2 µmol L^{-1}) with ZnMMTPP-MWCNT/GCE as the WE. (B) Calibration plot for the peak current data obtained in A. (C) DPV results for the intra-day study and (D) results for inter-day studies using 5, 20, and 40 µmol L^{-1} of NE in phosphate solution (pH 5.0) with ZnMMTPP-MWCNT/GCE. DPV parameters: a = 100 mV, t_m = 40 ms, ΔE = 3.0 mV, and t = 150 ms.

The analytical performance of the ZnMMTPP-MWCNT/GCE was compared with previously reported electrochemical methods for noradrenaline detection (Table S2). The sensor exhibited a LOD of 0.26 μM and a linear range of 1.0 – 84.2 μM, placing its analytical performance within the range of values reported for other modified electrodes. Although lower LODs have been reported for some materials (Table S2), these results demonstrate that the ZnMMTPP-MWCNT/GCE provides a suitable detection capability for NE. The relevance of this detection capability is supported by reported urinary NE concentrations of up to 6.0 μM in patients with phaeochromocytoma and acute heart failure [17]. Also, serum NE concentrations reported under severe pathological conditions exceeded the sensor LOD [19], indicating that the ZnMMTPP-MWCNT/GCE can detect NE at submicromolar concentrations within the range reported for such conditions.

Beyond the analytical figures of merit, the use of ZnMMTPP provides a functional contribution to the sensing interface. Metalloporphyrins benefit from coordination of additional ligands above and below the porphyrin plane, contributing to their catalytic efficiency in electrochemical sensing applications [37]. This feature is particularly relevant for the detection of biologically important molecules, such as neurotransmitters, which are important targets for electrochemical analysis [38]. In this context, electrochemical characterisation showed that the incorporation of zinc resulted in a two-fold increase in peak current compared with the metal-free porphyrin.

Intra- and inter-day repeatability studies were carried out for the ZnMMTPP-MWCNT/GC electrode, as shown in Figures 3C and 3D. These studies were conducted using three different concentrations of NE (5, 20, and 40 μmol L^{-1}), with three independently prepared electrodes over three consecutive days. The intra-day results demonstrated excellent reproducibility, with relative standard deviations (RSD) below 2 % for the anodic peak current and below 1 % for the anodic peak potential across three DPV measurements. Similarly, the inter-day repeatability showed good stability, with RSD values below 8 %. These results confirm the reliability and stability of the proposed electrode for noradrenaline detection. To assess the selectivity of noradrenaline detection using the ZnMMTPP-MWCNT/GC electrode, the influence of potential interfering species commonly found in biological fluids was evaluated using the DPV technique. The tested interferents included urea, glucose (GLU), ascorbic acid (AA), dopamine (DA), caffeine (CAF), uric acid (UA), and common ions such as chloride (Cl^-), sodium (Na^+), potassium (K^+), and sulphate (SO_4^{2-}). As shown in Figure S15 and Table S3, the presence of these species at a 10-fold excess relative to noradrenaline resulted in deviations of −7.3 % to +4.8 % in the measured current. The largest deviations were observed for uric acid (−7.3 %)

and ascorbic acid and dopamine (+4.8 %), whereas the other species produced only minor changes in the analytical response. Overall, the relatively small deviations observed under the tested conditions indicate that the proposed electrode is capable of maintaining its response to noradrenaline in the presence of the investigated potential interferents.

Finally, the ZnMMTPP-MWCNT/GCE was employed for the detection of noradrenaline in synthetic urine and serum samples. To evaluate its performance in complex matrices, spiked samples were analysed using the modified electrode, and the results are summarised in Table 2.

Table 2. Determination of noradrenaline in spiked synthetic urine and bovine serum using the ZnMMTPP-MWCNT/GC electrode

Sample[a]	[NE]		
	Added (μM)	Found (μM)	Recovery[b] (%)
Synthetic urine	2.0	1.8±0.03	90.0
	8.0	7.9±0.2	98.7
	25.0	25.0±0.5	100.0
Bovine serum	2.0	1.83±0.07	91.5
	8.0	7.87±0.02	98.4
	25.0	24.9±0.2	99.6

[a]n=3; [b]Recovery = ([NE]Found/[NE]Added)×100 %.

The recovery values obtained for noradrenaline, as presented in Table 2, ranged from 90.0 % to 100.0 % for spiked synthetic urine and bovine serum samples. For both matrices, recoveries were close to 100 % at the higher noradrenaline concentrations, ranging from 98.4 % to 100.0 %, whereas slightly lower recoveries were observed at the lowest concentration tested (90.0 % and 91.5 % for synthetic urine and bovine serum, respectively). Overall, these results indicate that the ZnMMTPP-MWCNT/GC electrode can provide satisfactory recovery of noradrenaline in the presence of the investigated sample matrices, supporting its potential applicability to the analysis of noradrenaline in complex samples.

Conclusions

In this study, a ZnMMTPP-MWCNT-modified glassy carbon electrode was successfully developed for the electrochemical determination of noradrenaline. The synthesis and incorporation of ZnMMTPP into the MWCNT-based film were confirmed by spectroscopic, mass spectrometric, microscopic, and elemental characterisation. The electrochemical results demonstrated that the porphyrin structure, particularly the presence of the Zn(II) centre, plays an important role in modulating the electron-transfer properties of the sensing interface. Compared with the metal-free porphyrin, incorporation of Zn resulted in a two-fold increase in the anodic peak current, together with a lower charge-transfer resistance (0.161 kΩ) and a higher apparent electron-transfer rate constant (1.7×10^{-3} cm s^{-1}), evidencing the contribution of ZnMMTPP to the facilitated interfacial electron transfer. The higher faradaic capacitance observed for the Zn-containing electrode further supports the interaction of noradrenaline with the porphyrin-based interface.

The resulting ZnMMTPP-MWCNT/GCE exhibited a linear response towards noradrenaline from 1.0 to 84.2 μmol L^{-1}, with a detection limit of 0.26 μmol L^{-1}. The electrode also showed satisfactory repeatability, with intra-day RSD values below 2 %, and recoveries ranging from 90.0 % to 100.0 % in spiked synthetic urine and bovine serum samples. Overall, these results demonstrate that combining the conductive properties of MWCNTs with the redox-active characteristics of a zinc metalloporphyrin provides a functional strategy for improving the electrochemical response towards noradrenaline. The findings therefore highlight the potential of ZnMMTPP as an active component of porphyrin-based electrochemical sensing interfaces for the detection of biologically relevant analytes.

Acknowledgements

The authors thank the funding agencies: Conselho Nacional de Desenvolvimento Científico e Tecnológico – CNPq (grant numbers 140406/2021-2 and 401681/2023-8), Fundação Coordenação de Aperfeiçoamento de Pessoal de Nível Superior – CAPES (finance code 001 and CAPES-Print 88887.836030/2023-00), and National Institute of Science and Technology of Nanomaterials for Life (INCT NanoVida) (CNPq grant 406079/2022-6). We thank the Laboratory of Structural Characterization (LCE/DEMa/UFSCar) for the general facilities and the Laboratory of Natural Product (LPN/UFSCar), especially PhD. Carlos André Ferreira Morais, for the mass spectrometry analyses.

Ethics declarations

Artificial Intelligence (AI)

Not Applicable.

Contributions

Karen Kenlderi de Lima Augusto: Methodology, conceptualization, investigation, validation, writing-original draft, and writing-review and editing. **Paulo Cardoso Gomes-Junior**: Methodology, conceptualization, investigation, validation, writing-original draft, and writing-review and editing. **Josias da Silveira Rocha**: Methodology, conceptualization, investigation, validation, and writing-review and editing. **Kleber Thiago de Oliveira**: Resources. **George Bueno Santana Pereira**: Methodology, conceptualization, investigation, validation, and writing-review and editing. **Orlando Fatibello-Filho**: Resources, supervision, and funding acquisition.

References

[1] L.M.C. Ferreira, P.S. Silva, K.K.L. Augusto, P.C. Gomes-Júnior, S.O.D. Farra, T.A. Silva, O. Fatibello-Filho, F.C. Vicentini, Using nanostructured carbon black-based electrochemical (bio)sensors for pharmaceutical and biomedical analyses: A comprehensive review, J. Pharm. Biomed. Anal. 221 (2022) 115032. https://doi.org/https://doi.org/10.1016/j.jpba.2022.115032.

[2] S.J. Malode, M.M. Shanbhag, R. Kumari, D.S. Dkhar, P. Chandra, N.P. Shetti, Biomass-derived carbon nanomaterials for sensor applications, J. Pharm. Biomed. Anal. 222 (2023) 115102. https://doi.org/10.1016/j.jpba.2022.115102.

[3] M. Sajid, J. Płotka-Wasylka, Nanoparticles: Synthesis, characteristics, and applications in analytical and other sciences, Microchemical Journal 154 (2020) 104623. https://doi.org/10.1016/j.microc.2020.104623.

[4] Q. Zhao, Z. Gan, Q. Zhuang, Electrochemical Sensors Based on Carbon Nanotubes, Electroanalysis 14 (2002) 1609–1613. https://doi.org/10.1002/elan.200290000.

[5] A. Nag, A. Mitra, S.C. Mukhopadhyay, Graphene and its sensor-based applications: A review, Sens. Actuators A Phys. 270 (2018) 177–194. https://doi.org/10.1016/j.sna.2017.12.028.

[6] M. Biesaga, K. Pyrzyn, M. Trojanowicz, Porphyrins in analytical chemistry. A review, Talanta 51 (2000) 209–224.

[7] J.E. Falk, Porphyrins and Metalloporphyrins, Elsevier, Amsterdam, 1975.

[8] D. Jemmeli, C. Mchiri, Development of a new bisphenol A electrochemical sensor based on a cadmium (II) porphyrin modified, RSC Adv. 10 (2020) 31740–31747. https://doi.org/10.1039/D0RA04793G.

[9] F. Rejab, N. Elhouda, D. Ahlem, R. Mosaab, E. Nicole, Highly Sensitive Electrochemical Sensor Based on Zn Porphyrin for Environmental Monitoring of Glyphosate, Electroanalysis 37 (2025) 1–10. https://doi.org/10.1002/elan.70037.

[10] Z.N. Siddiqui, S. Aqsa, B. Bukhari, H. Nasir, Fabrication of zinc tetramethoxyphenyl porphyrin-CNTs nanosensor for efficient sensing of the anticancer drug, 5-fluorouracil in human serum, Electrochim. Acta 531 (2025) 146453. https://doi.org/10.1016/j.electacta.2025.146453.

[11] T. Pradhan, H.S. Jung, J.H. Jang, T.W. Kim, C. Kang, J.S. Kim, Chemical sensing of neurotransmitters, ChemSocRev 43 (2014) 4684–4713. https://doi.org/10.1039/c3cs60477b.

[12] S. Askri, M. Moslah, H. Mkacher, H. Nasri, Development of a new electrochemical sensor for serotonin detection based on a manganese (III) porphyrin complex, Analytical Methods 17 (2025) 8212–8223. https://doi.org/10.1039/D5AY01128K.

[13] J. Ma, W. Bai, X. Liu, J. Zheng, Electrochemical dopamine sensor based on bi-metallic Co/Zn porphyrin metal – organic framework, Microchimica Acta (2022). https://doi.org/10.1007/s00604-021-05122-3.

[14] G. Fernandes, R. Lam, J. Park, G.T. Drummond, M. Sur, Noradrenaline Regulation of Brain-Body Communication, in: 2025: pp. 35–61. https://doi.org/10.1007/978-3-031-89525-8_2.

[15] J.W.M. Lenders, Q.-Y. Duh, G. Eisenhofer, A.-P. Gimenez-Roqueplo, S.K.G. Grebe, M.H. Murad, M. Naruse, K. Pacak, W.F. Young, Pheochromocytoma and Paraganglioma: An Endocrine Society Clinical Practice Guideline, J. Clin. Endocrinol. Metab. 99 (2014) 1915–1942. https://doi.org/10.1210/jc.2014-1498.

[16] A. van Berkel, J.W.M. Lenders, H.J.L.M. Timmers, DIAGNOSIS OF ENDOCRINE DISEASE: Biochemical diagnosis of phaeochromocytoma and paraganglioma, Eur. J. Endocrinol. 170 (2014) R109–R119. https://doi.org/10.1530/EJE-13-0882.

[17] K. Wang, J. Liang, S. Shen, Pheochromocytoma with acute heart failure as a complication—emphasis on the etiology of acute heart failure for diagnosis and treatment: a case report, BMC Cardiovasc. Disord. 25 (2025) 605. https://doi.org/10.1186/s12872-025-05044-5.
[18] Y.J. Chee, C.H.Y. Teo, R.T.M. Au, Y.C. Kon, Subclinical phaeochromocytoma: a diagnostic and management challenge, BMJ Case Rep. 15 (2022) e248571. https://doi.org/10.1136/bcr-2021-248571.
[19] K. Suzuki, T. Miyake, H. Okada, F. Yamaji, Y. Kitagawa, T. Fukuta, R. Yasuda, Y. Tanaka, H. Okamoto, S. Nachi, T. Doi, T. Yoshida, K. Kumada, S. Yoshida, H. Ushikoshi, I. Toyoda, S. Ogura, Thyrotoxic and pheochromocytoma multisystem crisis: a case report, J. Med. Case Rep. 11 (2017) 173. https://doi.org/10.1186/s13256-017-1299-y.
[20] J.S. Lindsey, I.C. Schreiman, H.C. Hsu, P.C. Kearney, A.M. Marguerettaz, Rothemund and Adler-Longo reactions revisited: synthesis of tetraphenylporphyrins under equilibrium conditions, J. Org. Chem. 52 (1987) 827–836. https://doi.org/10.1021/jo00381a022.
[21] G.B.S. Pereira, J.S. Rocha, M. V. Palmeira-Mello, T. Teixeira, C.A.F. Moraes, N.N.P. da Silva, J.L. Dutra, D.B. Fortaleza, I.C. Prescilio, P.H.O. Santiago, J.H. Araujo-Neto, M.R. Cominetti, J.A. Ellena, A.A. Batista, F. V. Rocha, Phototoxicity evaluation of tetra-cationic ruthenium-arene-phosphine porphyrins in ovarian tumor cells, Biomaterials Advances 187 (2026) 214953. https://doi.org/10.1016/j.bioadv.2026.214953.
[22] N. Laube, B. Mohr, A. Hesse, Laser-probe-based investigation of the evolution of particle size distributions of calcium oxalate particles formed in artificial urines, J. Cryst. Growth 233 (2001) 367–374. https://doi.org/10.1016/S0022-0248(01)01547-0.
[23] G.B.S. Pereira, J. da Silveira Rocha, M.A. Lima, G.P. de Oliveira, R.G. da Silveira, M.R. Forin, L. da Silva Pinto, K.T. de Oliveira, F.V. Rocha, An experimental and theoretical approach of coordination compounds derived from meso-tetra(thiophen-2-yl)porphyrin: DNA interactions and cytotoxicity, Inorg. Chem. Commun. 147 (2023) 110135. https://doi.org/https://doi.org/10.1016/j.inoche.2022.110135.
[24] J.S. McIndoe, K.L. Vikse, Assigning the ESI mass spectra of organometallic and coordination compounds, Journal of Mass Spectrometry 54 (2019) 466–479. https://doi.org/https://doi.org/10.1002/jms.4359.
[25] H. Beitollahi, F. Movahedifar, S. Tajik, S. Jahani, A Review on the Effects of Introducing CNTs in the Modification Process of Electrochemical Sensors, Electroanalysis 31 (2019) 1195–1203. https://doi.org/10.1002/elan.201800370.
[26] J. Ma, W. Bai, X. Liu, J. Zheng, Electrochemical dopamine sensor based on bi-metallic Co/Zn porphyrin metal–organic framework, Microchimica Acta 189 (2022) 20. https://doi.org/10.1007/s00604-021-05122-3.
[27] D. Jemmeli, C. Mchiri, C. Dridi, H. Nasri, E. Dempsey, Development of a new bisphenol A electrochemical sensor based on a cadmium(<scp>ii</scp>) porphyrin modified carbon paste electrode, RSC Adv. 10 (2020) 31740–31747. https://doi.org/10.1039/D0RA04793G.
[28] T. Pajkossy, Impedance spectroscopy at interfaces of metals and aqueous solutions — Surface roughness, CPE and related issues, Solid State Ion. 176 (2005) 1997–2003. https://doi.org/10.1016/J.SSI.2004.06.023.
[29] A. Bard, L. Faulkner, Electrochemical Methods: Fundamentals and Applications, Wiley, New York, 2001.
[30] Z. Galus, Fundamentals of electrochemical analysis, Ellis Horwood, New York, 1976.
[31] M. Mazloum-Ardakani, H. Beitollahi, M.A. Sheikh-Mohseni, H. Naeimi, N. Taghavinia, Novel nanostructure electrochemical sensor for electrocatalytic determination of norepinephrine in the presence of high concentrations of acetaminophene and

folic acid, Appl. Catal. A Gen. 378 (2010) 195–201. https://doi.org/10.1016/J.APCATA.2010.02.019.
[32] M. Mazloum-Ardakani, Z. Alizadeh, F. Sabaghian, B.B.F. Mirjalili, N. Salehi, Novel Fe2O3@CeO2 Coreshell-based Electrochemical Nanosensor for the Voltammetric Determination of Norepinephrine, Electroanalysis 32 (2020) 455–461. https://doi.org/10.1002/ELAN.201900454.
[33] M. Taei, G. Ramazani, Simultaneous determination of norepinephrine, acetaminophen and tyrosine by differential pulse voltammetry using Au-nanoparticles/poly(2-amino-2-hydroxymethyl-propane-1,3-diol) film modified glassy carbon electrode, Colloids Surf. B Biointerfaces 123 (2014) 23–32. https://doi.org/10.1016/j.colsurfb.2014.09.005.
[34] X. Ma, M. Chen, X. Li, A. Purushothaman, F. Li, Electrochemical Detection of Norepinephrine in the Presence of Epinephrine, Uric Acid and Ascorbic Acid Using a Graphene-modified Electrode, Int. J. Electrochem. Sci. 7 (2012) 991–1000. https://doi.org/10.1016/S1452-3981(23)13389-X.
[35] G.S. Pallam, S. Sam, S. S., K.G. Kumar, A sensitive voltammetric sensor for the simultaneous determination of norepinephrine and its co-transmitter octopamine using a biopolymer modified glassy carbon electrode, Ionics (Kiel). 29 (2023) 819–831. https://doi.org/10.1007/s11581-022-04848-1.
[36] M.G. Gopika, B. Sajeevan, A.S. Murali, S. lekshmi, M. Govindasamy, B. Saraswathyamma, A Surfactant-Electropolymer modified dual sensor for the monitoring of norepinephrine at nanomolar levels in biological samples and pharmaceutical formulations, Mater. Chem. Phys. 318 (2024) 129266. https://doi.org/10.1016/j.matchemphys.2024.129266.
[37] M. Biesaga, Porphyrins in analytical chemistry. A review, Talanta 51 (2000) 209–224. https://doi.org/10.1016/S0039-9140(99)00291-X.
[38] R. Paolesse, S. Nardis, D. Monti, M. Stefanelli, C. Di Natale, Porphyrinoids for Chemical Sensor Applications, Chem. Rev. 117 (2017) 2517–2583. https://doi.org/10.1021/acs.chemrev.6b00361.

Supplementary Files

This is a list of supplementary files associated with this preprint. Click to download.

- SImanuscriptPorphyrinNE.docx
- graphicalabstract.tif